Journal of Materials Chemistry A

PAPER

View Article Online
View Journal

Cite this: DOI: 10.1039/c4ta00958d

Photolithographic fabrication of high-performance all-solid-state graphene-based planar micro-supercapacitors with different interdigital fingers†

Zhong-Shuai Wu,[a] Khaled Parvez,[a] Xinliang Feng*[ab] and Klaus Müllen*[a]

Received 24th February 2014
Accepted 14th March 2014

DOI: 10.1039/c4ta00958d

www.rsc.org/MaterialsA

Here we demonstrated the fabrication of ultrahigh rate, all-solid-state, planar interdigital graphene-based micro-supercapacitors (MSCs) manufactured by methane plasma-assisted reduction and photolithographic micro-fabrication of graphene oxide films on silicon wafers. Notably, the electrochemical performance of MSCs is significantly enhanced by increasing the number of the interdigital fingers from 8 to 32 and minimizing the finger width from 1175 to 219 μm, highlighting the critical importance of adjusting the number and widths of the fingers in the fabrication of high-performance MSCs. The fabricated graphene-based MSCs delivered an area capacitance of 116 μF cm^{-2} and a stack capacitance of 25.9 F cm^{-3}. Furthermore, they offered a power density of 1270 W cm^{-3} that is much higher than that of electrolytic capacitors, an energy density of ~3.6 mW h cm^{-3} that is comparable to that of lithium thin-film batteries, and a superior cycling stability of ~98.5% capacitance retention after 50 000 cycles. More importantly, the microdevice can operate well at an ultrahigh scan rate of up to 2000 V s^{-1}, which is three orders of magnitude higher than that of conventional supercapacitors.

Introduction

The rapid development of miniaturized, wearable and implantable electronic devices has significantly increased the demand for micro-electrochemical energy storage devices.[1–5] Micro-supercapacitors (MSCs) as a novel class of micro/nano-scale power sources have attracted widespread attention due to their extremely short ion diffusion pathways.[6–8] In principle, MSCs can provide various unique features, such as an ultrahigh power density that is several orders of magnitude higher than that of batteries and conventional supercapacitors, a large rate capability, environmental safety, almost zero maintenance, and superior cycling lifetime (millions of cycles). MSCs offer sufficient peak power for numerous on-chip uses that can be directly coupled with micro-electromechanical systems, energy harvesting microdevices, energy storage units (micro-batteries and capacitors), micro-sensors, biomedical implants, and active radiofrequency identification tags.[8–11]

Graphene-based MSCs with an in-plane geometry have emerged as promising micro-electrochemical energy storage devices that can take full advantage of the planar device configuration and graphene for charge storage.[10,12] In contrast to conventional sandwich-type supercapacitors, graphene-based planar interdigital MSCs allow for making the entire device much thinner, smaller, and more flexible on any substrate.[12,13] The electrolyte ions are confined within narrow interspaces between the electrode fingers and can be readily transported to offer an ultrahigh power capability due to the short ion diffusion distance. The separator layer normally used in conventional supercapacitors is not required in MSCs.[14–17] Therefore, planar MSCs bear the merits of easy fabrication for micro-patterned electrodes, facile adjustment of the interspaces and electrode fingers in micro-patterns, and elaborated integration into electronics on the same substrate.[6] Significant advancement in graphene-based MSCs has been made through the fabrication of novel graphene-based materials (such as graphene sheets, graphene quantum dots, hybrids of graphene–carbon nanotubes, and graphene/MnO_2), and the development of thin-film micro-fabrication technologies.[9,10,12,18–23] However, further improvement of the electrochemical performance of MSCs through the elaborated adjustment of the number and widths of the interdigital fingers remains a great challenge.

To address this, here we describe the fabrication of ultrahigh rate, all-solid-state, planar, and interdigital graphene-based MSCs manufactured by methane plasma-assisted reduction and photolithographic micro-fabrication of graphene oxide (GO)

[a]Max-Planck-Institut für Polymerforschung, Ackermannweg 10, 55128 Mainz, Germany. E-mail: feng@mpip-mainz.mpg.de; muellen@mpip-mainz.mpg.de; Fax: +49 6131 379 350; Tel: +49 6131 379 150

[b]School of Chemistry and Chemical Engineering, Shanghai Jiao Tong University, 200240, Shanghai, P. R. China

† Electronic supplementary information (ESI) available: Supplementary figures, and calculation of specific capacitance, energy density and power density. See DOI: 10.1039/c4ta00958d

films on silicon wafers. The capacitance, rate capability, and power/energy densities of MSCs are greatly enhanced by increasing the number of fingers (from 8 to 32) and narrowing the finger width (from 1175 to 219 μm). The resultant binder-free graphene-based MSCs deliver an area capacitance of ~116 μF cm^{-2} and a stack capacitance of ~25.9 F cm^{-3}. Furthermore, they exhibit: a power density of 1270 W cm^{-3} at a discharge time of ~0.5 ms, much higher than that of electrolytic capacitors (10^2–10^3 W cm^{-3}); an energy density of ~3.6 mWh cm^{-3}, comparable to that of lithium thin-film batteries; and superior cycling stability (98.5% capacitance retention after 50 000 cycles). The discharge rate of the microdevices with significant capacitive behavior was measured up to 2000 V s^{-1}, three orders of magnitude higher than that of conventional supercapacitors.[24]

Experimental

Fabrication of all-solid-state graphene-based MSCs

First, GO was synthesized from natural flake graphite with the Hummers method, reported in our previous work.[25–27] Then, a stable GO dispersion (2.5 mg mL^{-1}) obtained after 2 h by sonication was spin-coated several times at 2000 rpm for 60 s (Headway Research Inc.) to achieve a desirable uniform GO film on the oxygen plasma-treated silicon wafer (300 nm SiO_2 layer, Si-Mat) using 150 W rf power for 10 min (Plasma System 200-G, Technics Plasma GmbH). Subsequently, the fabricated GO films were rapidly reduced at 700 °C for 20 s with the methane (CH_4) plasma (AIXTRON, Nanoinstruments Black Magic) at a heating rate of 50 °C min^{-1} to form the reduced GO films. The designed flow rate of CH_4 gas into a plasma chamber was ~100 sccm. The plasma was operated with a 15 kHz waveform drive, and ignited with a high-voltage of 800 V. The chamber pressure during plasma treatment was ~6.20 Torr. After that, standard photolithography techniques were used for patterning graphene micro-electrodes. Specially, a positive photoresist G1805 was spin coated on the surface of the graphene film at a speed of 4000 rpm for 30 s. The resulting photoresist film was soft baked for 60 s at 115 °C on a hot plate, and the baked photoresist film was patterned from a mask with a UV exposure (Karl Süss MJB3 Mask Aligner, vacuum contact) for 4 s. Hard bake thus was conducted for 60 s at 115 °C on a hot plate. After this, the sample was developed for 30 s in the ma-D330 developer. After photoresist rinsing in DI water and drying, a thin Au layer (30 nm, Premion, 99.9985% metals basis, Alfa Aesar) was deposited on their surface. The thermal evaporation rate of Au was controlled at ~1.0 Å s^{-1} and the chamber pressure was ~3.75×10^{-6} Torr (EDWARDS FL400). And the photoresist was lifted off in acetone with the assistance of sonication for several minutes. The resulting Au micro-patterns of the desired electrode geometry were produced and served as a protection mask against oxygen plasma etching (Plasma System 200-G, Technics Plasma GmbH, with 20 sccm O_2 flow and 100–200 W rf power under the vacuum of less than 0.05 mbar) of the graphene to create the patterns of graphene micro-electrodes on a SiO_2/Si wafer. Afterwards, 5 μL of a H_2SO_4–PVA gel electrolyte was carefully drop-cast onto the surface of interdigital electrodes and solidified overnight. Finally, one on-chip all-solid-state graphene-based MSC was achieved.

Materials characterization

Materials characterization were conducted by scanning electron microscopy (SEM, Gemini 1530 LEO), energy dispersive X-ray (EDX) and mapping analysis (Hitachi SU8000 SEM coupled with a Bruker XFlash Detector 5010), optical microscopy, atomic force microscopy (AFM, Veeco Dimension 3100), X-ray diffraction (XRD) patterns (SEIFERT XRD 3000 TT Bragg-Brentano diffractometer with Cu Ka radiation between 10° and 60° and an incident wavelength of 0.15418 nm), Raman spectra (Bruker, 532 nm) and X-ray photoelectron spectroscopy (XPS, Omicron Multiprobe equipped with the monochromatic Al Kα source, with an electron analyzer resolution of 0.9 eV). The electrical conductivity of the graphene film was measured by a standard four-point probe system with a Kiethley 2700 Multimeter.

Electrochemical measurement

Cyclic voltammetry (CV) tested at the scan rates of 0.01–2000 V s^{-1} and electrochemical impedance spectroscopy (EIS) recorded in the frequency range of 0.01–100 kHz with a 5 mV ac amplitude were carried out by a CHI 760D electrochemical workstation. The H_2SO_4–PVA gel electrolyte was prepared by mixing 6.0 g H_2SO_4 and 6.0 g PVA (M_w = 85 000–124 000, Sigma Aldrich) in 60 mL deionized water and heated at 80 °C for 1 h under vigorous stirring.[27] The detailed calculation of the specific capacitance, power density and energy density is shown in the ESI†.

Result and discussion

Fig. 1a illustrates the fabrication process of all-solid-state graphene-based, interdigital MSCs on a silicon wafer using a photolithography technique. First, a GO thin film was prepared by spin-coating a GO dispersion[25–27] (Fig. S1 in the ESI†) on a modified silicon wafer (with a 300 nm SiO_2 layer), which was treated with oxygen plasma before use (Steps 1 and 2). Next, the obtained GO film was rapidly reduced by methane (CH_4) plasma treatment at 700 °C for 20 s (Step 3). SEM and AFM images revealed large-area uniformity and continuity for the reduced graphene films, with a thickness of ~15 nm (Fig. 1b and c, and S2†). XRD, XPS, and four-point probe measurements further confirmed the efficient reduction of the graphene film with a *d*-spacing of ~3.36 Å, a high C/O ratio of ~9.2, and electrical conductivity of ~345 S cm^{-1} (Table S1, ESI†).[28] A standard photolithography technique was then applied to pattern the graphene micro-electrodes on the SiO_2/Si wafer. Briefly, a positive photoresist spin-coated on a graphene film was patterned using a custom-designed mask with UV exposure (Steps 4 and 5). After development (Step 6), an e-beam thermal evaporation was performed to deposit a thin Au layer on the surface (Step 7) and the remaining photoresist was lifted off in acetone with a short-term sonication (Step 8). The resulting patterned Au layer with the designed device configuration was then generated and acted as a protection mask against oxygen

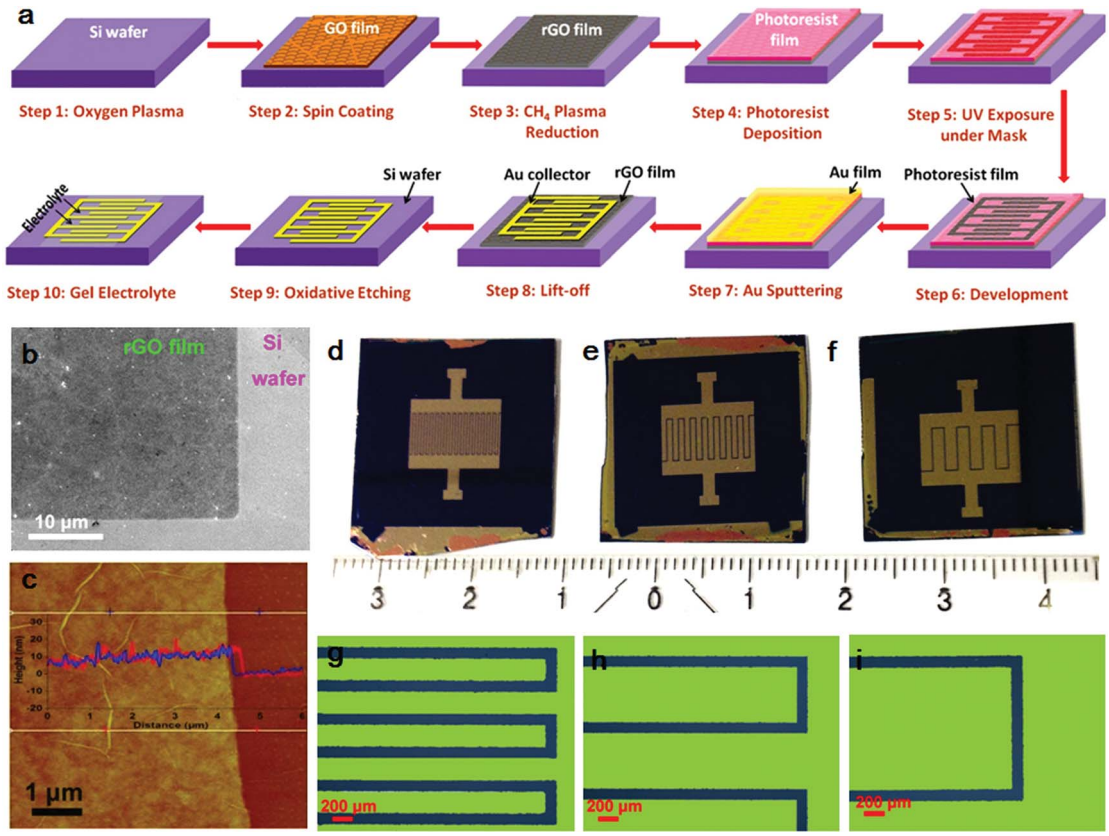

Fig. 1 (a) Schematic diagram of the fabrication of all-solid-state graphene-based planar MSCs on a silicon wafer fabricated using a photolithography technique. (b) SEM and (c) AFM images of methane plasma reduced GO (rGO) films. Inset in (c) is the height profile of the thickness of the fabricated film. (d–f) Optical images of graphene-based MSCs with an interdigital configuration with (d) 32 (MSCs(32)), (e) 16 (MSCs(16)), and (f) 8 (MSCs(8)) fingers. (g–i) Optical images of the fingers in (g) MSCs(32), (h) MSCs(16), and (i) MSCs(8).

plasma etching to manufacture the desired interdigital graphene electrode micro-patterns (Step 9). EDX elemental mapping analysis clearly reveals the uniform distribution of the Au element on the fingers and the Si element from the SiO_2 layer on the Si wafer along the interspace in the MSCs, and shows the smooth boundary between adjacent interspace and the fingers (Fig. S3†). Finally, a polymer gel electrolyte of H_2SO_4–polyvinyl alcohol (H_2SO_4–PVA) was drop-cast onto the interdigital electrode and allowed to solidify overnight (Step 10), thus achieving graphene-based interdigital MSCs with an in-plane geometry. By applying this procedure, graphene-based MSCs with different numbers of interdigital fingers (8, 16, and 32) were fabricated on the same total surface of the cell (Fig. S4†), and the corresponding microdevices were denoted as MSCs(8), MSCs(16), and MSCs(32), as shown in Fig. 1d–f. The widths of MSCs(8), MSCs(16), and MSCs(32) were 1175, 538, and 219 μm, respectively (Fig. 1g–i), while the widths of the interspaces between the fingers, the lengths of the fingers, and the thicknesses (~15 nm) of the graphene films were kept constant (Fig. S4†).

The electrochemical behavior of MSCs(32) was first examined by CV measurements at scan rates ranging from 0.01 to 2000 V s^{-1} (Fig. 2a–g) and galvanostatic charge and discharge curves at current densities from 1 to 400 μA cm^{-2} (Fig. S5†). Notably, MSCs(32) exhibited a typical electrical double-layer capacitive feature with a nearly rectangular CV shape, even at an ultrahigh scan rate of 1000 V s^{-1} (Fig. 2f), indicative of its extreme power capability. Remarkably, MSCs(32) allowed operation at an extremely high discharge rate, up to 2000 V s^{-1}, while maintaining excellent capacitance (Fig. 2g), which is characteristic of high instantaneous power. The rate of 2000 V s^{-1} is at least three orders of magnitude higher than that of conventional supercapacitors, and is the highest value for any high power MSCs reported to date (see Table S2, ESI†). Furthermore, MSCs(32) displayed excellent cycling stability, *e.g.*, ~98.5% of the initial capacitance (~20.6 μF cm^{-2}) was maintained after 50 000 cycles at a large scan rate of 100 V s^{-1} (Fig. S6†).

To evaluate the influence of the number and width of the fingers on the electrochemical performance of graphene-based MSCs(32), MSCs(16) (Fig. S7†), and MSCs(8) (Fig. S8†) with different numbers of interdigital fingers were investigated further. The maximum scan rate of MSCs(32) was up to ~2000 V s^{-1}, much higher than those of MSCs(8) (~100 V s^{-1}) and MSCs(16) (~300 V s^{-1}) (Fig. 2h). Accordingly, MSCs(32) delivered a higher discharge current than MSCs(8) and MSCs(16) at a given scan rate. For example, at a scan rate of 200 V s^{-1}, discharge currents of 0.19, 0.47, and 0.95 mA were obtained for

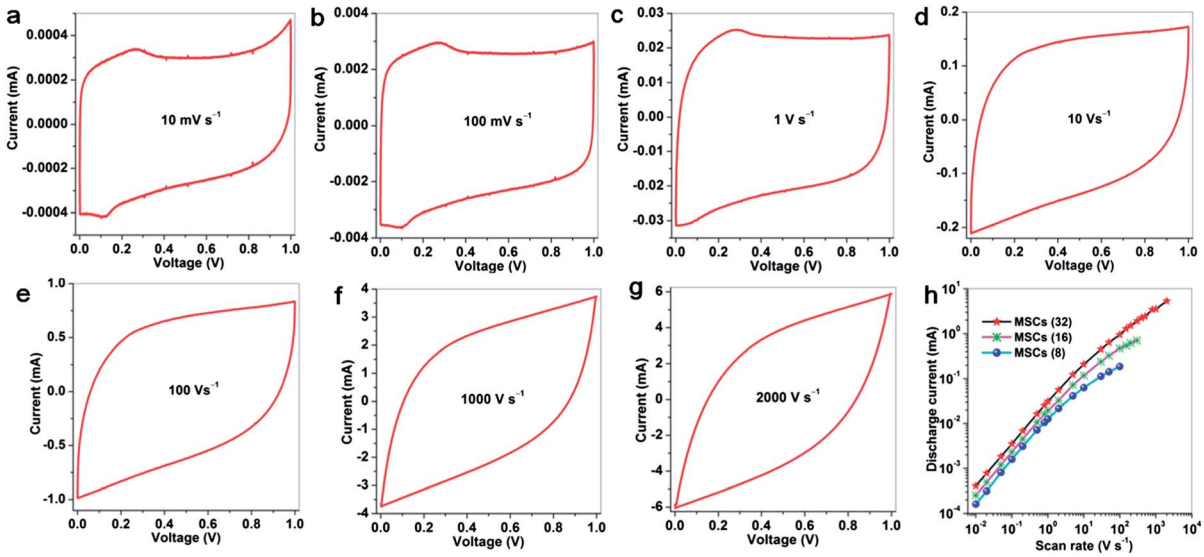

Fig. 2 (a–g) CV curves of graphene-based MSCs(32) obtained at different scan rates of (a) 0.01, (b) 0.1, (c) 1, (d) 10, (e) 100, (f) 1000, and (g) 2000 V s^{-1}. (h) A plot of the discharge current as a function of scan rate for MSCs(8), MSCs(16) and MSCs(32).

MSCs(8), MSCs(16) and MSCs(32), respectively. This result suggests that the greater the number of fingers in the MSCs, the higher the scan rate (or discharge current), and thus more power could be extracted from the microdevices. Increasing the finger number or narrowing the finger width efficiently decreases the average ionic diffusion pathway between the adjacent fingers, and consequently reduces the electrolyte resistance with low ion transport limitations.[15] This result further highlights the crucial role of the device architecture in determining the electrochemical performance of MSCs.

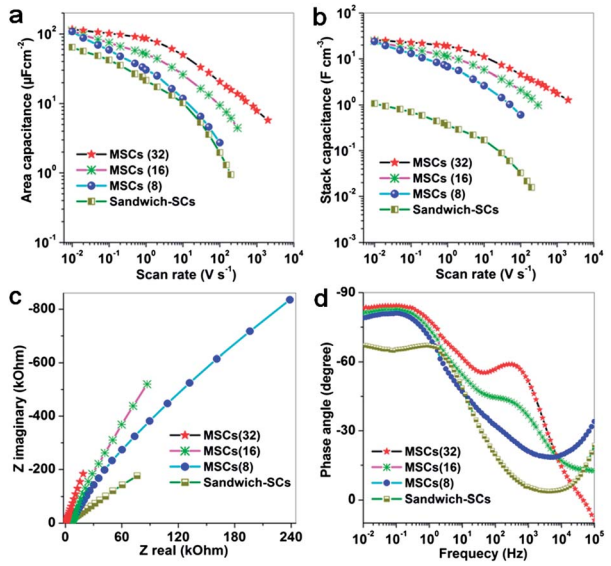

Fig. 3 (a and b) Comparison of (a) area capacitance and (b) stack capacitance of graphene-based MSCs(32), MSCs(16), MSCs(8), and sandwich-SCs as a function of scan rate. (c and d) Comparison of (c) Nyquist plot and (d) impedance phase angle *vs.* the frequency of graphene-based MSCs(32), MSCs(16), MSCs(8), and sandwich-SCs.

The area capacitance and stack capacitance of graphene-based MSCs(8), MSCs(16), and MSCs(32) are shown in Fig. 3a and b. For comparison, graphene-based sandwich-supercapacitors (denoted as sandwich-SCs) are also included in the plots. At a low scan rate of 10 mV s^{-1}, the area capacitance and stack capacitance of MSCs(32) were calculated to be ~116 μF cm^{-2} and ~25.9 F cm^{-3}, respectively, which were higher than those of MSCs(16) (~111 μF cm^{-2} and ~24.7 F cm^{-3}) and MSCs(8) (~108 μF cm^{-2} and ~24.0 F cm^{-3}). Moreover, the rate capability of MSCs(32) outperforms those of MSCs(16) and MSCs(8). Upon increasing the scan rates, the capacitance of MSCs(32) slowly declines. In this case, an area capacitance of ~20.6 μF cm^{-2} and a stack capacitance of ~4.6 F cm^{-3} were maintained at 100 V s^{-1}. Even at an ultrafast scan rate of 2000 V s^{-1}, MSCs(32) still retained an area capacitance of ~5.7 μF cm^{-2} and a stack capacitance of ~1.3 F cm^{-3}. In sharp contrast, area capacitance and stack capacitance of ~4.5 μF cm^{-2} and ~1.0 F cm^{-3}, respectively, were provided for MSCs(16) at 300 V s^{-1}, and ~2.7 μF cm^{-2} and ~0.6 F cm^{-3}, respectively, for MSCs(8) at 100 V s^{-1}. Thereby, it can be concluded that, on a given total area, (i) narrowing the width of the fingers in MSCs can shorten the ion diffusion pathway, and (ii) increasing the number of the fingers in MSCs can increase the length of the interface between the active-material electrode and the electrolyte, thus contributing to the improved double-layer storage and enhanced rate capability of MSCs. On the other hand, sandwich-SCs with the H_2SO_4–PVA gel electrolyte between two MPG film (~15 nm) electrodes were examined. The obtained area, stack capacitances (~64 μF cm^{-2} and ~1.1 F cm^{-3}) and rate capability (~2.0 μF cm^{-2} and ~0.03 F cm^{-3} at 100 V s^{-1}) for sandwich-SCs were much lower than those of the above three MSCs with different numbers of interdigital fingers, suggesting the superiority of the in-plane geometry over the stack geometry for the enhancement of electrochemical performance.[13] Additionally, the largest scan

rate (~200 V s^{-1}) of sandwich-SCs observed was higher than that (100 V s^{-1}) of MSCs(8), possibly due to the long ion diffusion pathway of the MSCs(8) (>1175 μm).

We next investigated the electrochemical impedance of graphene-based MSCs(32), MSCs(16), MSCs(8), and sandwich-SCs, as shown in Fig. 3c. Remarkably, the Nyquist plots of MSCs(32) exhibited a larger slope at a low frequency, which was closer to the *Y*-axis than those of MSCs(16) and MSCs(8), indicating better electrical double layer capacitive behavior in MSCs with a greater number of interdigital fingers. In addition, the slopes of all three microdevices were superior to those of sandwich-SCs, further emphasizing the importance of device geometry in capacitive performance.

The phase angle as a function of the frequency for MSCs(32), MSCs(16), MSCs(8), and sandwich-SCs is presented in Fig. 3d. The characteristic frequency f_0 at a phase angle of −45° was ~1572 Hz for MSCs(32), which was much higher than that of MSCs(16) (~69 Hz), MSCs(8) (~15 Hz), and sandwich-SCs (~13 Hz). Based on the equation[7] $\tau_0 = 1/f_0$ (time constant τ_0 is defined as the minimum time to discharge all of the energy from the device with an efficiency of more than 50%), the corresponding time constant τ_0 was calculated to be ~0.64 ms for MSC(32), suggesting fast accessibility of the ions within the MSCs(32). In sharp contrast, MSCs(16), MSCs(8) and sandwich-SCs had much larger τ_0 values of 14.5, 66.7, and 76.9 ms, respectively, at a −45° phase angle.

For evaluation of the energy and power densities of MSCs(8), MSCs(16), and MSCs(32), a Ragone plot is shown in Fig. 4. Data from sandwich-SCs, a commercial high-energy thin-film lithium battery (4 V/500 μA h),[7] and a high power aluminium electrolytic capacitor (3 V/300 μF)[29] are included for comparison. Increasing the number of interdigital fingers remarkably improved both the energy and power densities of MSCs, especially within a short discharge time from seconds to milliseconds. For example, MSCs(32) delivered a volumetric energy density of ~3.6 mW h cm^{-3}, which was higher than those of MSCs(8) (~3.3 mW h cm^{-3}) and MSCs(16) (~3.4 mW h cm^{-3}). Notably, this value was well comparable to that of lithium thin-film batteries (1–10 mW h cm^{-3}).[7] Furthermore, MSCs(32) offer an ultrahigh power density of 1270 W cm^{-3} discharged within an extremely short time of ~0.5 ms, superior to those of MSCs(8) (~30 W cm^{-3} for 10 ms discharge) and MSCs(16) (~140 W cm^{-3} for 3.3 ms discharge). It should be emphasized that the power density of ~1270 W cm^{-3} is the highest value for any state-of-the-art ultrahigh power MSCs reported to date (Table S2, ESI†),[6,7,9] and is three orders of magnitude higher than that of the conventional supercapacitors (<10 W cm^{-3}), and even superior to that of high power electrolytic capacitors (10^2 ~ 10^3 W cm^{-3}).[29]

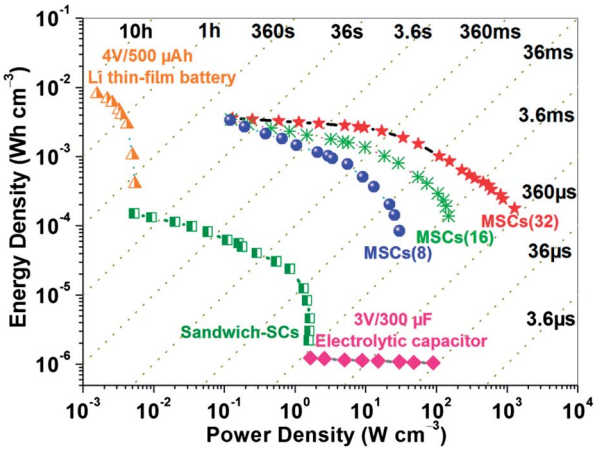

Fig. 4 Ragone plot of all-solid-state, graphene-based MSCs(32), MSCs(16), MSCs(8), and sandwich-SCs in comparison with the well-known electrolytic capacitors[29] and lithium thin-film batteries.[7]

Conclusion

We described all-solid-state, graphene-based, planar MSCs fabricated using a photolithography technique. The resultant microdevices showed exceptional electrochemical performance, including high area and stack capacitance, ultrahigh scan rate, ultrahigh power and energy densities, and superior cycling stability. We speculate that the performance of the graphene-based MSCs can be enhanced by further miniaturization of the finger width and the interspaces between adjacent fingers. Such graphene-based MSCs have great potential as nano/micro-scale power sources for integrating numerous miniaturized electronics and other on-chip applications.

Acknowledgements

This work was financially supported by ERC grants on NANOGRAPH and 2DMATER, DFG Priority Program SPP 1459, EU Projects GENIUS, UPGRADE and Graphene Flagship (no. CNECT-ICT-604391).

Notes and references

1 P. Simon and Y. Gogotsi, *Nat. Mater.*, 2008, **7**, 845–854.
2 D. R. Rolison, R. W. Long, J. C. Lytle, A. E. Fischer, C. P. Rhodes, T. M. McEvoy, M. E. Bourga and A. M. Lubers, *Chem. Soc. Rev.*, 2009, **38**, 226–252.
3 M. Koo, K. I. Park, S. H. Lee, M. Suh, D. Y. Jeon, J. W. Choi, K. Kang and K. J. Lee, *Nano Lett.*, 2012, **12**, 4810–4816.
4 L. B. Hu, J. W. Choi, Y. Yang, S. Jeong, F. La Mantia, L. F. Cui and Y. Cui, *Proc. Natl. Acad. Sci. U. S. A.*, 2009, **106**, 21490–21494.
5 M. Kaempgen, C. K. Chan, J. Ma, Y. Cui and G. Gruner, *Nano Lett.*, 2009, **9**, 1872–1876.
6 J. Chmiola, C. Largeot, P. L. Taberna, P. Simon and Y. Gogotsi, *Science*, 2010, **328**, 480–483.
7 D. Pech, M. Brunet, H. Durou, P. H. Huang, V. Mochalin, Y. Gogotsi, P. L. Taberna and P. Simon, *Nat. Nanotechnol.*, 2010, **5**, 651–654.
8 Z. S. Wu, X. L. Feng and H. M. Cheng, *Natl. Sci. Rev.*, 2013, DOI: 10.1093/nsr/nwt1003.
9 W. Gao, N. Singh, L. Song, Z. Liu, A. L. M. Reddy, L. J. Ci, R. Vajtai, Q. Zhang, B. Q. Wei and P. M. Ajayan, *Nat. Nanotechnol.*, 2011, **6**, 496–500.
10 M. F. El-Kady and R. B. Kaner, *Nat. Commun.*, 2013, **4**, 1475.

11 W. Si, C. Yan, Y. Chen, S. Oswald, L. Han and O. G. Schmidt, *Energy Environ. Sci.*, 2013, **6**, 3218–3223.
12 Z. S. Wu, G. M. Zhou, L. C. Yin, W. C. Ren, F. Li and H. M. Cheng, *Nano Energy*, 2012, **1**, 107–131.
13 J. J. Yoo, K. Balakrishnan, J. S. Huang, V. Meunier, B. G. Sumpter, A. Srivastava, M. Conway, A. L. M. Reddy, J. Yu, R. Vajtai and P. M. Ajayan, *Nano Lett.*, 2011, **11**, 1423–1427.
14 J. H. Sung, S. J. Kim, S. H. Jeong, E. H. Kim and K. H. Lee, *J. Power Sources*, 2006, **162**, 1467–1470.
15 D. Pech, M. Brunet, T. M. Dinh, K. Armstrong, J. Gaudet and D. Guay, *J. Power Sources*, 2013, **230**, 230–235.
16 J. Feng, X. Sun, C. Z. Wu, L. L. Peng, C. W. Lin, S. L. Hu, J. L. Yang and Y. Xie, *J. Am. Chem. Soc.*, 2011, **133**, 17832–17838.
17 D. Pech, M. Brunet, P. L. Taberna, P. Simon, N. Fabre, F. Mesnilgrente, V. Conedera and H. Durou, *J. Power Sources*, 2010, **195**, 1266–1269.
18 Z. Weng, Y. Su, D. W. Wang, F. Li, J. H. Du and H. M. Cheng, *Adv. Energy Mater.*, 2011, **1**, 917–922.
19 M. Beidaghi and C. L. Wang, *Adv. Funct. Mater.*, 2012, **22**, 4501–4510.
20 L. L. Peng, X. Peng, B. R. Liu, C. Z. Wu, Y. Xie and G. H. Yu, *Nano Lett.*, 2013, **13**, 2151–2157.
21 W. W. Liu, X. B. Yan, J. T. Chen, Y. Q. Feng and Q. J. Xue, *Nanoscale*, 2013, **5**, 6053–6062.
22 J. Lin, C. G. Zhang, Z. Yan, Y. Zhu, Z. W. Peng, R. H. Hauge, D. Natelson and J. M. Tour, *Nano Lett.*, 2013, **13**, 72–78.
23 Z. Q. Niu, L. Zhang, L. L. Liu, B. W. Zhu, H. B. Dong and X. D. Chen, *Adv. Mater.*, 2013, **25**, 4035–4042.
24 J. R. Miller and P. Simon, *Science*, 2008, **321**, 651–652.
25 Z. S. Wu, Y. Sun, Y. Z. Tan, S. B. Yang, X. L. Feng and K. Müllen, *J. Am. Chem. Soc.*, 2012, **134**, 19532–19535.
26 Z. S. Wu, S. B. Yang, Y. Sun, K. Parvez, X. L. Feng and K. Müllen, *J. Am. Chem. Soc.*, 2012, **134**, 9082–9085.
27 Z. S. Wu, A. Winter, L. Chen, Y. Sun, A. Turchanin, X. Feng and K. Müllen, *Adv. Mater.*, 2012, **24**, 5130–5135.
28 Z. S. Wu, K. Parvez, X. L. Feng and K. Müllen, *Nat. Commun.*, 2013, **4**, 2487.
29 M. F. El-Kady, V. Strong, S. Dubin and R. B. Kaner, *Science*, 2012, **335**, 1326–1330.

